Electronic supplementary information (ESI)

Chemicals and handling

All chemicals were of reagent grade and used as received. Ethanol was used without any further purification. All manipulations were made under aerobic conditions. The mother solution was filtered over ashless paper and solid crystals were collected on fritted glass with porosity no 4. $Ni(SCN)_2$ was prepared via an exchange reaction of $NiCl_2 \cdot 6H_2O$ and KSCN in ethanol.

Physical Measurements

Element content of C, H, N and S in the complex was determined by microanalytical method (Thermo Electron Flash Elemental Analyzer 1112). Melting point was studied with thermo-microscopy by Kofler hot-stage microscope at $4°C \cdot min^{-1}$ until 300°C and reported without corrections. The solid sample for FT-IR measurements was not dried and it was used as freshly synthesized. The spectrum was acquired on Attenuated total reflection (ATR) holder with effective diamond crystal in the region of 4000 - 400 cm^{-1} (Nicolet 5700, Thermo Electron). Electronic spectrum of triturated powder sample in mineral oil was collected in region 9000 - 50 000 cm^{-1} (Specord 200, Analytical Jena).

Preparation of $[Ni(NCS)_2(nqu)_2(H_2O)_2] \cdot 2nqu$ (1)

A 100 cm^3 round bottom flask was charged with 5-nitroquinoline (0.150 g, 0.86 mmol) and dissolved in ethanol (10 cm^3). The mixture was enriched by greenish ethanol solution (2 cm^3) of $Ni(SCN)_2$ (0.075 g, 0.43 mmol). The reaction mixture was heated with an oil bath for 4 hours at 80 °C. Small green crystals were obtained by a slow evaporation from the saturated liquid at the ambient temperature in four days. Yield: 0.165 g, 42%. Melting point: 140-142 °C. *Anal. Calc*. for $C_{38}H_{28}N_{10}NiO_{10}S_2$ (907.53 $g \cdot mol^{-1}$): C, 50.29; H, 3.11; N, 15.43; S, 7.07. Found: C, 49.95; H, 2.95; N, 15.35; S, 7.11 %. Selected FT-IR bands (ATR) ν/cm^{-1}: 3377, 3116, 3064, 2098(s), 1595, 1516(s), 1417(m), 1345(m), 1316(m), 1217, 1145(m), 1068, 985, 879(s), 835(m), 802, 791(s), 751, 735(m), 662, 637, 584, 544, 507, 455, 416 (s – strong, m – medium). UV/Vis (Nujol) $\nu_{max}/10^3$ cm^{-1} (relat. absorb.): 9.940(0.239); 15.504(0.251); 16.42(0.292); 18.116(0.407); 18.975(0.433); 19.763(0.426); 26.042(0.334).

Spectroscopic characterization

The solid state ATR/FT-IR spectra of the complex **1** were measured at ambient temperature. The sharp band with strong intensity at the 2098 cm^{-1} proves an asymmetric stretching frequency ν_{as} of –N=C=S group (Fig. S1).

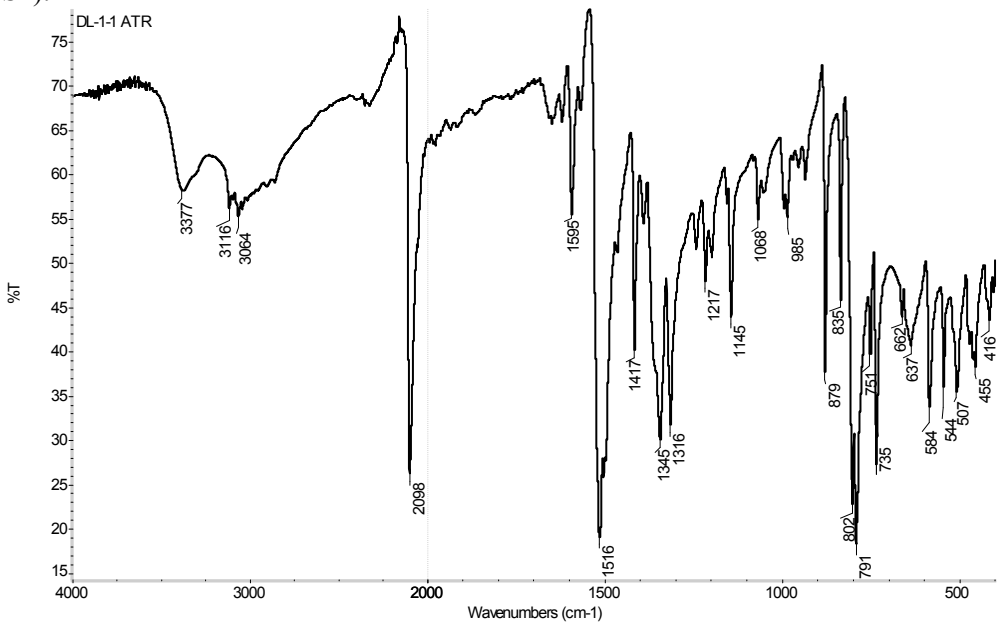

Figure S1. FT-IR spectrum of **1** (400 – 4000 cm^{-1}).

The UV/Vis spectrum of **1** taken in the Nujol suspension shows two of three spin allowed d-d bands $^3T_{2g} \leftarrow {}^3A_{2g}(F)$ and $^3T_{1g} \leftarrow {}^3A_{2g}(F)$ of week intensity between 9 000 – 18 000 cm^{-1}; the third band $^3T_{1g}(P) \leftarrow {}^3A_{2g}(F)$ is masked by a charge-transfer band above 22 000 cm^{-1} (Fig. S2). Moreover, influence of spin-orbit coupling manifests itself in an appearance of the spin forbidden band $^1E_g \leftarrow {}^3A_{2g}$ of low intensity between 12 000-14 000 cm^{-1}.

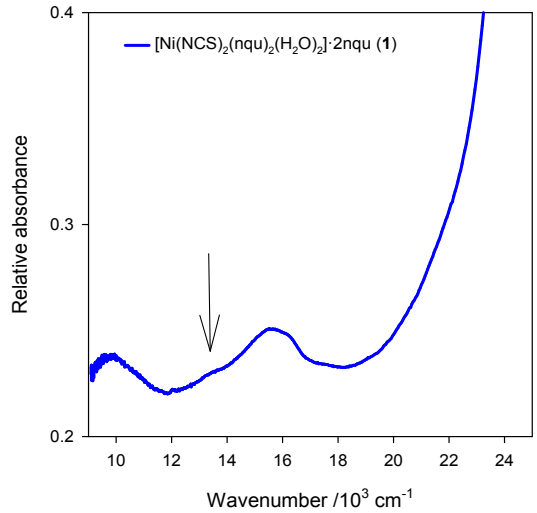

Figure S2. Electronic spectrum of **1** taken in the Nujol suspension. An arrow indicates the spin forbidden band.

Table S1. Crystal data for **1**

	1
Empirical formula	$C_{38}H_{28}N_{10}NiO_{10}S_2$
Formula weight /g mol^{-1}	907.53
Crystal system	triclinic
Space group	*P*–1
Temperature /K	100(1)
Crystal size /mm	0.35 × 0.16 × 0.08
Z	1
a / Å	8.0112(3)
b / Å	8.0734(3)
c / Å	14.9981(5)
α /°	82.284(3)
β /°	81.302(3)
γ /°	76.188(3)
V /Å^3	926.28(6)
Calculated density D_c /g cm^{-3}	1.627
Absorption coefficient μ /mm^{-1}	2.473
Reflections collected /unique	22071/3495
Final R indices [I≥2σ(I)	R_1 = 0.0314
	wR_2 = 0.0883
R indices (all data)	R_1 = 0.0351
	wR_2 = 0.0899

Table S2. Selected bonds (Å) and angles (°) in **1**

Ni1–O1W	2.078(1)	Ni1–O1W^i	2.078(1)
Ni1–N1	2.214(1)	Ni1–N1^i	2.214(1)
Ni1–N2	2.031(1)	Ni1–N2^i	2.031(1)
O1W–Ni1–O1W^i	180.0	O1W^i–Ni1–N1^i	93.17(4)
O1W–Ni1–N1^i	86.84(4)	O1W–Ni1–N1	93.16(4)
O1W^i–Ni1–N1	86.83(3)	N1–Ni1–N1^i	180.0
N2^i–Ni1–O1W^i	86.41(5)	N2–Ni1–O1W	86.41(5)
N2^i–Ni1–O1W	93.59(5)	N2–Ni1–O1W^i	93.59(5)
N2^i–Ni1–N1^i	87.45(5)	N2–Ni1–N1^i	92.56(5)
N2^i–Ni1–N1	92.55(5)	N2–Ni1–N1	87.45(5)
N2–Ni1–N2^i	180.0		

Symmetry code: (*i*) 1–x, 2–y, –z.

Table S3. Hydrogen bonds (Å,°) in **1**

D–H···A	*d*(D–H)	*d*(H–A)	*d*(D–A)	D–H–A
O1W–H1WA···S1^{ii}	0.84	2.39	3.213(1)	167
O1W–H1WB···N4	0.84	1.94	2.770(2)	169

Symmetry code: (*ii*) 1–x, 2–y, –z.

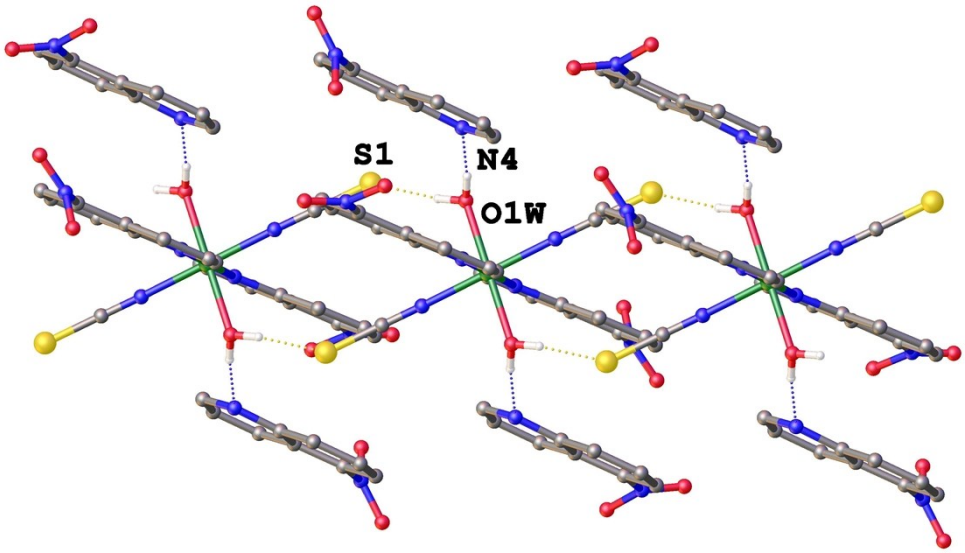

Figure S3. The supramolecular chain in **1**.

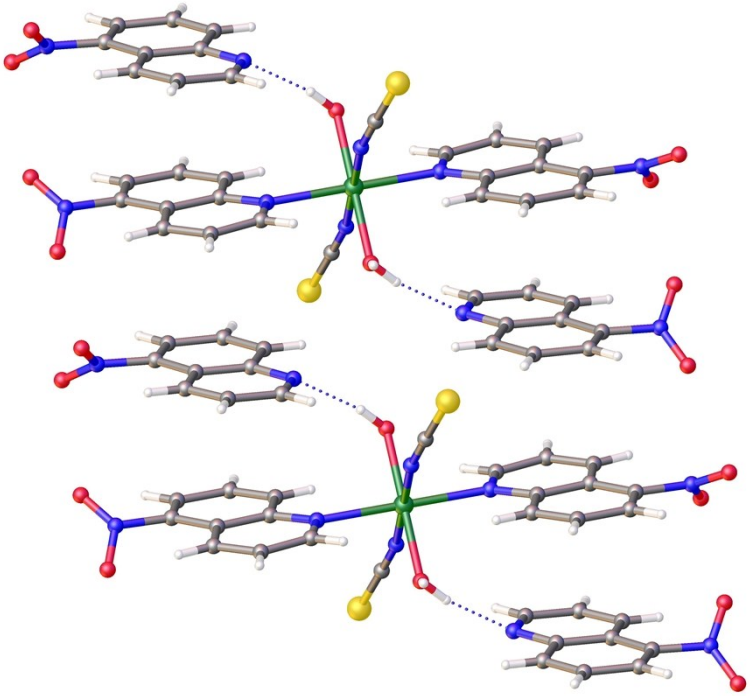

Figure S4. The π–π stacking in **1**.

Table S4. Individual contributions to D-tensor by *ab initio* (ORCA) calculations

Block	Mult	Root	D	E
0	3	0	-0.000	0.000
0	**3**	**1**	**-48.953**	**0.543**
0	**3**	**2**	**18.611**	**10.880**
0	**3**	**3**	**20.444**	**-11.778**
0	3	4	0.293	-0.198
0	3	5	0.145	0.250
0	3	6	0.135	-0.123
0	3	7	0.003	0.013
0	3	8	0.020	-0.022
0	3	9	0.004	0.002
1	1	0	-0.003	0.003
1	1	1	-0.002	0.002
1	**1**	**2**	**14.798**	**-0.112**
1	**1**	**3**	**-6.812**	**5.554**
1	**1**	**4**	**-6.355**	**-5.310**
1	1	5	-0.004	0.003
1	1	6	-0.201	-0.231
1	1	7	-0.163	0.180
1	1	8	-0.009	-0.002
1	1	9	-0.074	0.049
1	1	10	0.586	-0.246
1	1	11	-0.109	0.200
1	1	12	-0.663	0.346
1	1	13	0.044	-0.311
1	1	14	-0.000	0.000

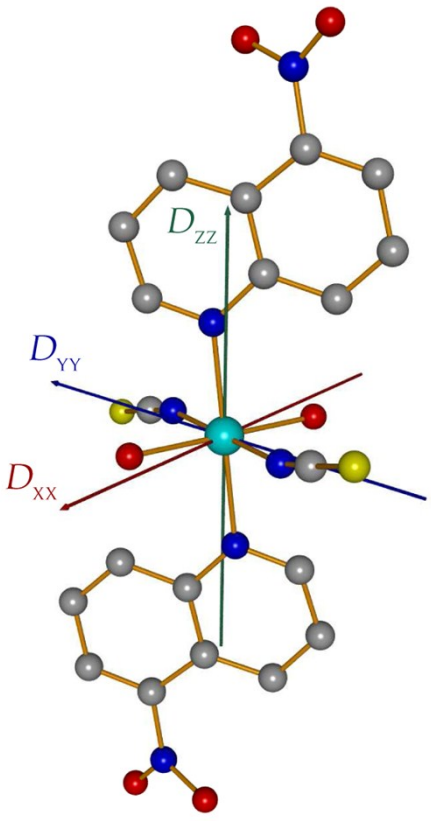

Figure S5. Orientation of the principal D-tensor components in the complex.

AC susceptibility data

A general formula for the complex AC susceptibility is

$$\chi(\omega) = \chi_S + \sum_{k=1}^{N} \frac{\chi_k - \chi_{k-1}}{1 + (\mathrm{i}\omega\tau_k)^{1-\alpha_k}}, \quad \omega = 2\pi f, \quad \chi_0 = \chi_S$$

For the **three-set Debye model** the following relationships hold true

$$\chi(\omega) = \chi_S + \frac{\chi_{T1} - \chi_S}{1 + (\mathrm{i}\omega\tau_1)^{1-\alpha_1}} + \frac{\chi_{T2} - \chi_{T1}}{1 + (\mathrm{i}\omega\tau_2)^{1-\alpha_2}} + \frac{\chi_{T3} - \chi_{T2}}{1 + (\mathrm{i}\omega\tau_3)^{1-\alpha_3}} \text{ or}$$

$$\chi(\omega) = \chi_S + (\chi_T - \chi_S)\left[\frac{x_1}{1 + (\mathrm{i}\omega\tau_1)^{1-\alpha_1}} + \frac{x_2}{1 + (\mathrm{i}\omega\tau_2)^{1-\alpha_2}} + \frac{x_3}{1 + (\mathrm{i}\omega\tau_3)^{1-\alpha_3}}\right], \quad x_3 = 1 - x_1 - x_2$$

a) the in-phase component

$$\chi'(\omega) = \chi_S + (\chi_{T1} - \chi_S)\frac{1 + (\omega\tau_1)^{1-\alpha_1}\sin(\pi\alpha_1/2)}{1 + 2(\omega\tau_1)^{1-\alpha_1}\sin(\pi\alpha_1/2) + (\omega\tau_1)^{2-2\alpha_1}}$$
$$+(\chi_{T2} - \chi_{T1})\frac{1 + (\omega\tau_2)^{1-\alpha_2}\sin(\pi\alpha_2/2)}{1 + 2(\omega\tau_2)^{1-\alpha_2}\sin(\pi\alpha_2/2) + (\omega\tau_2)^{2-2\alpha_2}}$$
$$+(\chi_{T3} - \chi_{T2})\frac{1 + (\omega\tau_3)^{1-\alpha_3}\sin(\pi\alpha_3/2)}{1 + 2(\omega\tau_3)^{1-\alpha_3}\sin(\pi\alpha_3/2) + (\omega\tau_3)^{2-2\alpha_3}}$$

b) the out-of-phase component

$$\chi''(\omega) = (\chi_{T1} - \chi_S)\frac{(\omega\tau_1)^{1-\alpha_1}\cos(\pi\alpha_1/2)}{1 + 2(\omega\tau_1)^{1-\alpha_1}\sin(\pi\alpha_1/2) + (\omega\tau_1)^{2-2\alpha_1}}$$
$$+(\chi_{T2} - \chi_{T1})\frac{(\omega\tau_2)^{1-\alpha_2}\cos(\pi\alpha_2/2)}{1 + 2(\omega\tau_2)^{1-\alpha_2}\sin(\pi\alpha_2/2) + (\omega\tau_2)^{2-2\alpha_2}}$$
$$+(\chi_{T3} - \chi_{T2})\frac{(\omega\tau_3)^{1-\alpha_3}\cos(\pi\alpha_3/2)}{1 + 2(\omega\tau_3)^{1-\alpha_3}\sin(\pi\alpha_3/2) + (\omega\tau_3)^{2-2\alpha_3}}$$

The mole fractions fulfil

$(\chi_{T1} - \chi_S) = (\chi_T - \chi_S)x_1$, $(\chi_{T2} - \chi_{T1}) = (\chi_T - \chi_S)x_2$, $(\chi_{T3} - \chi_{T2}) = (\chi_T - \chi_S)x_3$, $\chi_{T3} = \chi_T$

$x_1 = (\chi_{T1} - \chi_S)/(\chi_T - \chi_S)$, $x_2 = (\chi_{T2} - \chi_{T1})/(\chi_T - \chi_S)$, $x_3 = (\chi_{T3} - \chi_{T2})/(\chi_T - \chi_S)$

Table S5. Relaxation time for the low-frequency (LF) mode in **1**.

B_{DC}/T	T/K	$\tau_{LF}/10^{-3}$ s
0.4	1.9	275(23)
0.4	2.2	326(29)
0.4	2.3	328(51)
0.6	1.9	273(20)
0.8	1.9	270(18)
1.0	1.9	291(14)
1.2	1.9	336(37)
1.4	1.9	266(22)

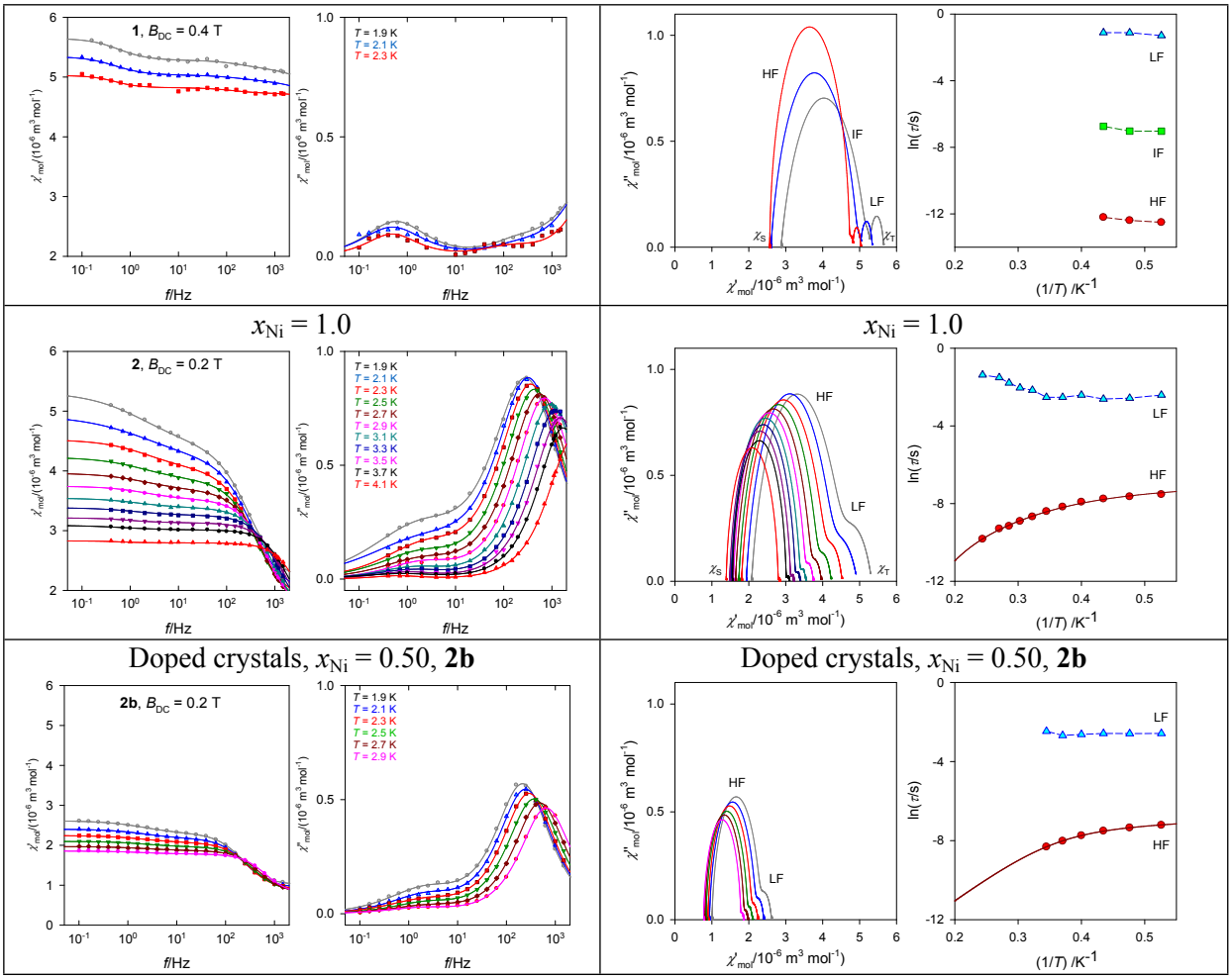

Figure S6. Comparison of AC susceptibility data for two hexacoordinate Ni(II) SIMs:
1 – [Ni(NCS)$_2$(*nqu*)$_2$(H$_2$O)$_2$]·2*nqu* (this work).
2 – [Ni(*pydc*)(*pydm*)]·H$_2$O (J. Miklovič, D. Valigura, R. Boča and J. Titiš, *Dalton Trans*., 2015, **44**, 12484).

DC magnetic data

Temperature dependence of the DC magnetization has been acquired with a SQUID magnetometer (MPMS-XL7, Quantum Design) using the RSO mode of detection. For magnetic susceptibility the applied field was $B_{DC} = 0.1$ T and this was corrected for the underlying diamagnetism and converted to the effective magnetic moment (Fig. S6). The magnetization data was taken at $T = 2.0$ and 4.6 K until $B = 7$ T.

In analyzing the DC magnetic data the zero-field splitting model applicable to a geometry of compressed tetragonal pyramid was used; this deals with two Kramers doublets and it is parameterized by the axial zero-field splitting parameter $D > 0$ and $g_e = g_z < g_x$

$$\hat{H}_{kl}^{\mathrm{zfs}} = D(\hat{S}_z^2 - \hat{S}^2/3)\mathsf{h}^{-2} + \hat{H}_{kl}^{Z} \qquad (1)$$

with the anisotropic Zeeman term defined by grids distributed uniformly over one hemisphere

$$\hat{H}_{kl}^{Z} = \mu_B B(g_z \hat{S}_z \cos\vartheta_k + g_x \hat{S}_x \sin\vartheta_k \cos\varphi_l + g_y \hat{S}_y \sin\vartheta_k \sin\varphi_l)\mathsf{h}^{-1} \qquad (2)$$

Its eigenvalues enter the partition function and consequently the formulae of the statistical thermodynamics for the magnetic susceptibility and magnetization. The magnetic field was oriented along 120 grids distributed uniformly over one hemisphere; this guarantees a correct powder average even when the D-parameter is large.

The magnetic data (temperature dependence of the molar magnetic susceptibility and field dependence of the molar magnetization at two temperatures) were fitted simultaneously by using a joint functional

$$F = w \cdot E(\chi) + (1 - w) \cdot E(M) \qquad (3)$$

where relative errors of susceptibility $E(\chi)$ and magnetization $E(M)$ are equally weighted. Corrections for the temperature-independent magnetism χ_{TIM} and a molecular field (zj) are effective to the high-temperature and low-temperature data, respectively

$$\chi' = \chi/[1 - (zj)\chi] + \chi_{TIM} \qquad (4)$$

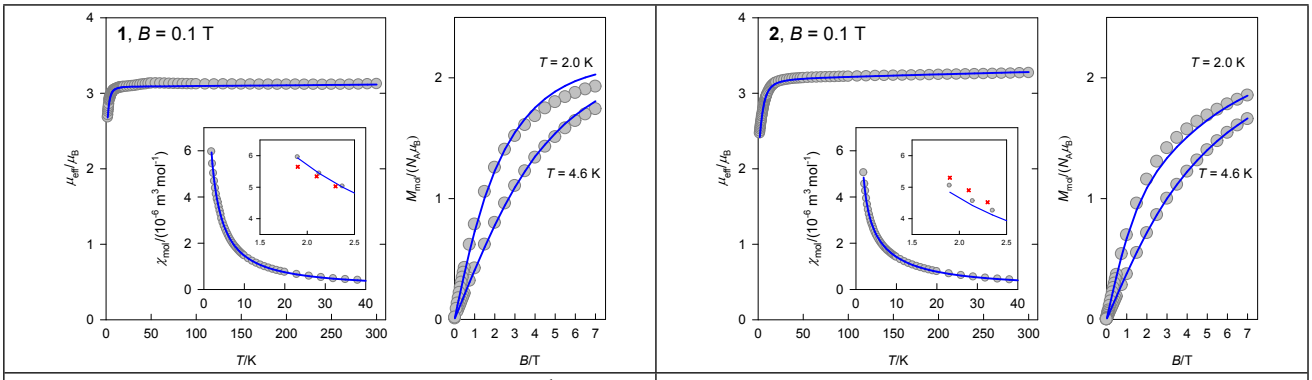

$g_{iso} = 2.180(27)$, $D/hc = -5.86(69)$ cm^{-1}, $zj/hc = 0.020$ cm^{-1}, $\chi_{TIM} = 0.99 \times 10^{-9}$ m^3 mol^{-1}	$g_x = 2.277$, $g_z = 2.289$ ($g_{iso} = 2.281$), $D/hc = -12.5$ cm^{-1}, $J/hc = 0.25$ cm^{-1}

Figure S7. DC magnetic data for **1** and **2**. Circles – experimental data; lines – fitted with the standard spin Hamiltonian model. Red crosses in the second inset: uncorrected, averaged AC susceptibility data in the low-frequency limit ($f = 0.01$ Hz).